Available online at www.sciencedirect.com
ScienceDirect
Journal of Power Sources 163 (2006) 420–432
JOURNAL OF POWER SOURCES
www.elsevier.com/locate/jpowsour

Non-linear dynamic modeling of proton exchange membrane fuel cell

Ahmad Haddad*, Rachid Bouyekhf, Abdellah El Moudni, Maxime Wack

Laboratoire Systèmes et Transports UTBM, Site de Belfort, Belfort Technopôle, 90010 Belfort Cedex, France

Received 9 May 2006; received in revised form 11 September 2006; accepted 12 September 2006
Available online 27 October 2006

Abstract

This paper proposes a non-linear state-space dynamic model for planar proton exchange membrane fuel cell (PEMFC). Our objective is the realization of a model that evokes a more realistic approach of dynamic behavior of the fuel cell by considering most of elements that influence the system evolution. For instance, pressure, temperature and humidification rate effects on the cell resistance are taken into account. The model is based on both thermodynamic and electrical aspects, proposing a realistic equivalent circuit which integrates most of the fuel cell components. Simulation results show that our proposed model is in agreement with fuel cell real operating principles.

Keywords: PEMFC; Dynamic modeling; Non-linear systems

1. Introduction

Since the decrease of the oil reserves, due to the massive exploitation of the fuel, the domain of energy becomes the focus of public interest. In addition, the environmental pollution requires the development of new technologies of energy. Given these facts, the fuel cell becomes a prime candidate as an energy source and a natural alternative, which gives innovating answers concerning the energy effectiveness.

In this paper, we study the proton exchange membrane fuel cell (PEMFC) which is considered as the most appropriate type of fuel cell for replacing internal combustion engines. It uses a solid polymer membrane (originally the Nafion 117) as electrolyte and usually works at average temperature (in the range of 40–90 °C). Compared to other types of fuel cells, PEMFC is more compact and lightweight because it generates a better volumic-power and power-density. In addition, its operating temperature is less than 100 °C, allowing rapid start-up. These facts and the ability to rapidly change power output are some of characteristics that make PEMFC suitable for automotive power applications. Other advantages result from the solid nature of the electrolyte because with a solid electrolyte the sealing of anode and cathode gases is far easier, and therefore, less expensive to manufacture. It has also less problems with corrosion, which means a longer cell and stack life.

There are several studies in the literature related to the PEMFC modeling. These studies aim at understanding the phenomena occurring in the fuel cell in order to make the appropriate control. A number of mathematical models have been developed for this purpose but they are mostly steady-state models which are typically used for component sizing [1,2], thermodynamical aspect [3–6] and electrical models [7,8]. These models represent each component such as compressor, heat exchanger and fuel cell stack voltage as a static performance or efficiency map. Another interesting model is the one developed by [9]. Based on the linearized Nernst potential, the authors have presented a simple basic isothermal cell model which is independent of the type of fuel cell and is used for a general description of cells with gaseous fuel.

While the above studies have been stated only for steady-state modeling, equivalent work have been presented for the dynamical modeling. Indeed, [10] uses the state-space linear form while [11] uses the Bond Graph method to model each component alone.

In summary, a large amount of literature has been published about modeling of PEMFCs but most of them are centered on either static electrochemical or linear dynamic aspect. However, non-linear dynamic characteristics of fuel cell must be modeled in order to ensure a better dynamic control which is suitable for dynamic applications such as vehicles propulsion. With the best

* Corresponding author. Tel.: +33 384583352; fax: +33 384583342.
E-mail address: ahmad.haddad@utbm.fr (A. Haddad).

0378-7753/$ – see front matter © 2006 Elsevier B.V. All rights reserved.
doi:10.1016/j.jpowsour.2006.09.012

Nomenclature

A	area (m^2)
C	concentration ($mol\,m^{-3}$)
C_{dl}, C_{geom}	double layer and geometrical capacity (F)
D	diffusion coefficient ($m^2\,s^{-1}$)
E	Nernst voltage (V)
F	Faraday constant = $96500\,C\,mol^{-1}$
ΔG	Gibbs free energy ($kJ\,mol^{-1}$)
i	output current cell (A)
j	current, density ($A\,cm^{-2}$)
J	diffusion flux ($\mu mol\,s^{-1}\,m^{-2}$)
J^r	consumption rate at triple phase boundary ($\mu mol\,s^{-1}$)
J^s	consumption rate flowing into the outer surface of the diffusion layer ($\mu mol\,s^{-1}$)
L	thickness (m)
M	molar mass ($g\,mol^{-1}$)
n	number of exchanged electrons
p, P	partial and total pressure (Pa)
r	pore radius (cm)
R	resistance (Ω)
R_g	gas constant = $8.314\,J\,(mol\,K)^{-1}$
s	Laplace operator
T	temperature (K)
u	inputs vector
v	auxiliary input
V	voltage (V)
V_e	electrode voltage (V)

Greek letters

α	charge transfer coefficient = 1
ϵ	porosity
η	voltage loss (V)
λ_m	humidification rate
σ	electrolyte conductivity $(\Omega\,m)^{-1}$
τ	tortuosity

Subscripts

a	anode
act	activation
c	cathode
conc	concentration
ct	charge transfer
load	load
m	membrane
o	ohmic
out	output

Superscripts

b	gas flow bulk
tpb	triple phase boundary
0	at standard pressure

of our knowledge, a notable work that takes into account this inherent non-linearity is the one given by [12]. In that paper, the authors present a cell-level non-linear state-space dynamic model of solid oxide fuel cell (SOFC). However, their model do not take into account the activation loss, the evolution of some parameters as well as the temperature evolution and the membrane humidity. They consider that electrochemical reaction potential, ohmic resistance and charge transfer resistance are constants while they depend respectively on pressures, humidification rate, temperature and current.

We propose in this paper a non-linear state-space dynamic model for single cell of a planar PEMFC structure that takes into account the influence of several parameters on the system behavior. Our model is based on both thermodynamic and electric aspects. On the one hand, the diffusion principle, which is drawn from [12], is used to describe pressures and flow rates evolutions. On the other hand, the electrical principle is used to model the voltage and the current. The dynamic behaviors of voltage, current and gas consumption rates are stated with respect to load, partial pressures, humidification rate and temperature. Furthermore, a more realistic equivalent circuit which integrates most of the fuel cell components is also proposed.

The remainder of this paper is organized as follows: Section 2 explains the PEMFC principle and states some known results and remarks, which are needed in the subsequent development. Section 3 presents a way to build the dynamic model of a single PEM-type cell. Finally, simulation results and analysis are discussed in Section 4.

2. Fuel cell principle

In this section, we describe the PEMFC principle from reaction equation and we point to the electrochemical equations as well as the voltage losses and current evolution. Indeed, a fuel cell is an electrochemical energy conversion device which produces electricity, water and heat using fuel and oxygen in the air. It is interesting to notice that water is the only emission when hydrogen is the fuel. The principle of PEMFC is shown in Fig. 1.

At the anode, the hydrogen molecule is split into hydrogen ions (protons) and electrons. The hydrogen ions permeate across the electrolyte to the cathode while the electrons flow through an external circuit and produce electric power. Oxygen, usually in the form of air, is supplied to the cathode and combines with electrons and hydrogen protons to produce water. Electrons circulation between anode and cathode through an external circuit generates electricity. The reaction that takes place at the triple phase boundary zone (TPB), is described as follows:

$$H_2 + \tfrac{1}{2}O_2 \longrightarrow H_2O + \text{electricity} + \text{heat}. \quad (1)$$

At standard pressure, each element of the fuel cell (a single cell) makes the direct transformation of chemical energy (Gibbs free energy) to electrical energy according to the following equation:

$$\Delta G + nFE^0 = 0. \quad (2)$$

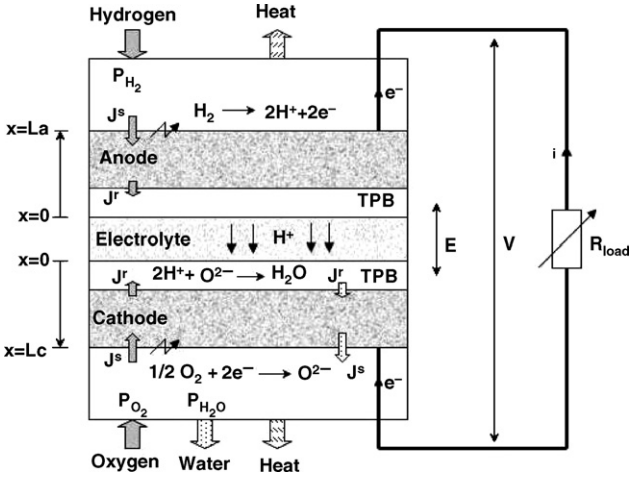

Fig. 1. Principle of PEMFC.

with $n = 2$ in this case, because the reaction involves two electrons.

Output voltage of the fuel cell is an important part of its modeling. At normal conditions of pressure and temperature, the electrochemical reaction potential is given by the Nernst equation [13]:

$$E = E^0 + H \ln\left(\frac{p_{H_2}\sqrt{p_{O_2}}}{p_{H_2O}}\right), \tag{3}$$

where $H = R_g T/nF$ and $E^0 = 1.273 - 2.7645 \times 10^{-4} T$.

When a fuel cell operates, the actual voltage is lower than the one computed with Nernst's equation, due to activation, diffusion and ohmic losses. The reduction of the voltage is proportional to the current circulation through the cell. Fig. 2 shows the voltage/current characteristic taking into account losses [14].

Fig. 2 shows three evolution zones for the output voltage:

- The first zone represents the activation loss caused by the charge transfer between electrodes and electrolyte. It appears only for a little current and is governed by the following equation:

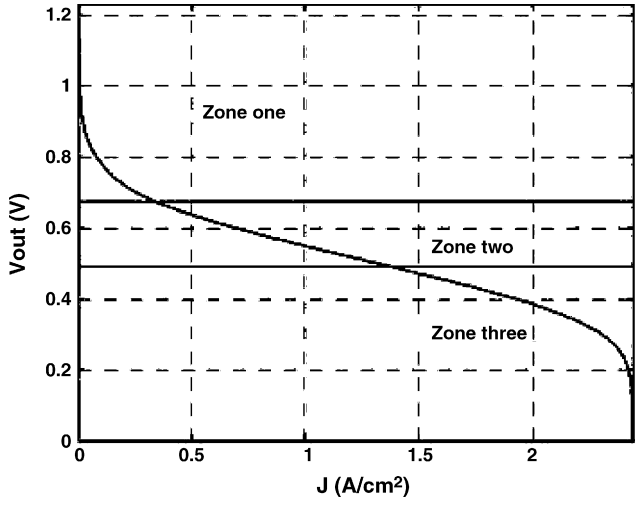

Fig. 2. Polarization curve.

$$\eta_{act} = \frac{R_g T}{\alpha n F} \ln\left(\frac{j}{j_0}\right), \tag{4}$$

where j_0 denotes exchange current density.

- The second zone represents the ohmic loss due to the resistance of different components of the fuel cell. Its expression is as follows:

$$\eta_o = R_o i_t, \tag{5}$$

where i_t is the total current.

- The third zone represents the concentration loss due to the mass transfer of reagents. It appears only for a huge current and is governed by the following equation:

$$\eta_{conc} = \frac{R_g T}{\alpha n F} \ln\left(1 - \frac{j}{j_l}\right), \tag{6}$$

where j_l denotes limit current density.

Hence, the effective output voltage of the fuel cell is given by the following equation:

$$V_{out} = E - \eta_{act} - \eta_o - \eta_{conc}. \tag{7}$$

Now, concerning the current output, the thermodynamic aspect of the fuel cell allows us to establish the relation between current and gas flow rates as follows [15]:

$$i_t = 2FJ^r_{H_2} = 2FJ^r_{H_2O} = 4FJ^r_{O_2}. \tag{8}$$

It is interesting to note that the current is not only influenced by load value but it depends on another variables. This fact can be easily seen in Eq. (8) which shows that current depends on gas flow rate and thus on gas pressures values. Besides, the current is limited by the maximum flow rate value which in turn depends on concentration gradients between TPB and gas flow bulks. When the current output increases, the hydrogen and oxygen concentrations at TPB decrease to create larger concentration gradients. However, because the cathode reaction is slower than the anode one, current output is also limited by the maximum ion production rate. In addition, the current is influenced by the membrane resistance which depends on the temperature and the humidification rate.

3. Modeling approach

In general, two types of fuel cell models have been considered in the literature: steady-state and dynamic models. The former focuses on simulating the fuel cell polarization curve while the latter generally pays more attention to thermodynamic aspects. This paper deals with modeling the dynamic performances of a fuel cell focusing on both electrical and diffusion approaches. The dynamics of the PEMFC will be represented by non-linear differential equations transformed into an equivalent mathematical formulation: the state-space representation. The method of state-space domain exhibits great advantages especially in the study of control, parameter estimation, data reconciliation and optimization. Besides, it presents a powerful tool for simulation.

As mentioned in Section 1, we are interested on the planar fuel cell geometry. This structure is built by stacking together multiple single cell. Hence, the fuel cell stack is electrically a

Table 1
Input/output variables

Inputs		Outputs	
$u_1 = R_{load}$	Load resistance	$y_1 = V_{out}$	Voltage output
$u_2 = p^b_{H_2}$	Partial pressure of hydrogen in anode gas bulk	$y_2 = i$	Current output
$u_3 = p^b_{O_2}$	Partial pressure of oxygen in cathode gas bulk	$y_3 = J^s_{H_2}$	Hydrogen consumption rate
$u_4 = p^b_{H_2O}$	Partial pressure of water vapor in anode gas bulk	$y_4 = J^s_{O_2}$	Oxygen consumption rate
$u_5 = \lambda$	Humidification rate	$y_5 = J^s_{H_2O}$	Water consumption rate
$u_6 = T$	Fuel cell temperature		

serial connection of these cells. It is basically this fact which motivates us to focus on a single cell modeling since in a serial connection the single cell voltage is added up. In addition, we consider that the fuel cell lies in a mesoscopic scale. For this reason, we may consider a single cell as a lumped volume type 0D of the stack. This enables us to assume an uniform variation of the temperature inside the single cell. However, it is important to note that the study of temperature variation with respect to the space scale needs a special thermal study which is not the subject of the paper.

According to these hypothesis, we develop a model based on diffusion and electrical principles. The diffusion principle enables us to identify pressures and flow rates while electrical principle allows us to model the voltage and the current. The PEMFC modeling process will be divided into three parts. In the first part, we establish relations between pressures and flow rates according to concentration and diffusion laws. Then, we set electrical relationships between voltage and current in the second part. The third part is devoted to the state-space formulation. To do this, we define in Table 1 the input/output variables.

The first input is the external load that influences the current output i and so affects the reaction. In order to investigate the basic dynamic behavior of the current output, load impedance is assumed to be a pure resistance R_{load} in the model. Other inputs are partial pressures of reactants in gas bulks. They affect the diffusion processes as well as the Gibbs free energy and thus the voltage and current outputs. The fifth input is the humidification rate λ related to the water management. Its role is to maintain the membrane humidity and to balance water usage/consumption in the system. Indeed, on one hand, much water leads to the flooding of the membrane, which in turn blocks the mass diffusion and proton transportation. On the other hand, if the humidification level of the membrane is too low, the proton transportation through the membrane will become difficult and this will lead to higher internal resistance. Another input that influences the membrane resistance is the temperature T which together with humidification rate influences the ohmic losses. This eventually affects voltage and current outputs. Finally, the output variables are voltage, current and gases consumption rates.

3.1. Diffusional approach

In this part, we are going to use the diffusion principle in order to establish the expressions of gas partial pressures p^{tpb} at TPB and gas consumption rate J^s at gas bulk. As the gas consumption rate J^r at TPB can be expressed with respect to the current (see Eq. (8)) and p^b is taken as an input variable, we will establish the expressions of p^{tpb} and J^s with respect to both p^b and J^r. Indeed, in our planar geometrical model for which the co-flow circulation of gases is considered, we determine the diffusion flux due to the concentration difference between gas bulk and TPB zones according to Fick's first law:

$$J = -D\nabla C, \tag{9}$$

where ∇C is the concentration gradient. The low diffusion layer thickness and the porous characteristic of the electrodes allow us to assume that gases diffuse in one dimension (in the x direction; see Fig. 1). Hence, the expression of the diffusion flux Eq. (9) becomes:

$$J = -D\frac{\partial C}{\partial x}. \tag{10}$$

The diffusion coefficient D in porous materials can be calculated according to Giavazzi–Pagano simplified equation:

$$D = 9700\, r\frac{\epsilon}{\tau}\sqrt{\frac{T}{M}}$$

In order to compute J we use Fick's second law which provides us the variation of the concentration with respect to time:

$$\frac{\partial C}{\partial t} = D\frac{\partial^2 C}{\partial x^2}. \tag{11}$$

For the solution of this equation, as in [12], we use the Laplace transforms which appears to be more suitable for the state-space representation. Indeed, the Laplace transforms of Eq. (11) is given by

$$\frac{\mathrm{d}^2 C(s)}{\mathrm{d}x^2} - \frac{s}{D}C(s) = 0. \tag{12}$$

with the following boundary conditions:

$$\begin{aligned} J^r(s) &= -AD\left.\frac{\mathrm{d}C(s)}{\mathrm{d}x}\right|_{x=0} \\ J^s(s) &= -AD\left.\frac{\mathrm{d}C(s)}{\mathrm{d}x}\right|_{x=L} \\ C^b(s) &= C(s)|_{x=L} \end{aligned} \tag{13}$$

Hence, the solution of Eq. (12) with respect to these boundary conditions is as follows:

$$\begin{aligned} C(s)(x) = &-\frac{J^r(s)\,\sinh(\sqrt{s/D}x)}{AD\sqrt{s/D}} \\ &+ \frac{J^r(s)\,\sinh(\sqrt{s/D}L) + C^b(s)AD\sqrt{s/D}}{AD\sqrt{s/D}\,\cosh(\sqrt{s/D}L)} \\ &\times \cosh\left(\sqrt{\frac{s}{D}}x\right). \end{aligned} \tag{14}$$

Now, assume that gases are ideal. Then we have:

$$P\mathcal{V} = NR_gT \Longrightarrow P = \frac{NR_gT}{\mathcal{V}} = CR_gT, \tag{15}$$

where N is the number of moles of gas present on the volume $\mathcal{V}$. At TPB we have $x = 0$ (see Fig. 1). This infers that $p^{\mathrm{tpb}}(s) = RTC(s)|_{x=0}$. With this in mind, from Eq. (14) we derive:

$$C(s)(0) = \frac{J^{\mathrm{r}}(s)}{AD\sqrt{s/D}}\left[\frac{\sinh(\sqrt{s/D}L)}{\cosh(\sqrt{s/D}L)} - 1\right] + \frac{C^{\mathrm{b}}(s)}{\cosh(\sqrt{s/D}L)}.$$

This and the fact that $p^{\mathrm{b}}(s) = RTC^{\mathrm{b}}(s)|_{x=0}$ imply:

$$p^{\mathrm{ptb}}(s) = \frac{RT}{AD\sqrt{s/D}}\left[\frac{\sinh(\sqrt{s/D}L)}{\cosh(\sqrt{s/D}L)} - 1\right] J^{\mathrm{r}}(s) + \frac{p^{\mathrm{b}}(s)}{\cosh(\sqrt{s/D}L)}. \tag{16}$$

Now, at the gas bulk zone we have $x = L$. It follows after a simple calculation that

$$J^{\mathrm{s}}(s) = \frac{J^{\mathrm{r}}(s)}{\cosh(\sqrt{s/D}L)} + \frac{AD\sqrt{s/D}}{RT}\tanh\left(\sqrt{\frac{s}{D}}L\right) p^{\mathrm{b}}(s). \tag{17}$$

As in [12], since L is around zero, the use of the Taylor's serie expansions of cosh, sinh and tanh functions about 0 and neglecting higher order terms we arrive at:

$$\begin{aligned} p^{\mathrm{tpb}}(s) &= G_{Jp}\, J^{\mathrm{r}}(s) + G_{pp}\, p^{\mathrm{b}}(s), \\ J^{\mathrm{s}}(s) &= G_{JJ}\, J^{\mathrm{r}}(s) + G_{pJ}\, p^{\mathrm{b}}(s), \end{aligned} \tag{18}$$

where

$$G_{Jp} = \frac{-(L/D) - (L^3/6D^2)s}{1 + (L^2/2D)s + (L^4/24D^2)s^2}\frac{RT}{A};$$

$$G_{pp} = \frac{1}{1 + (L^2/2D)s + (L^4/24D^2)s^2}$$

$$G_{JJ} = \frac{1}{1 + (L^2/2D)s + (L^4/24D^2)s^2};$$

$$G_{pJ} = \frac{Ls}{1 + (L^2/2D)s + (L^4/24D^2)s^2}\frac{A}{RT}$$

3.2. Electrical approach

It is by now well known that representing the fuel cell system as an electrical circuit is quite useful and a great effort has been made to assimilate the fuel cell to an inherent impedance by modeling the electrical effects of its components. According to the PEMFC principle (Section 2), fuel cell's voltage output is affected by gas partial pressures and is reduced by activation, concentration and ohmic losses. Because reactions take place at TPB, the more appropriate expression of Nernst equation is:

$$E = E^0 + H\,\ln\left(\frac{p^{\mathrm{tpb}}_{\mathrm{H_2}}\sqrt{p^{\mathrm{tpb}}_{\mathrm{O_2}}}}{p^{\mathrm{tpb}}_{\mathrm{H_2O}}}\right) \tag{19}$$

The electrochemical phenomena produced inside the fuel cell components are modeled by electric impedances. The inherent impedance is the equivalent circuit of these components. It represents the losses and its dynamic characteristics affect the dynamic behaviors of voltage and current. More precisely, it is composed of:

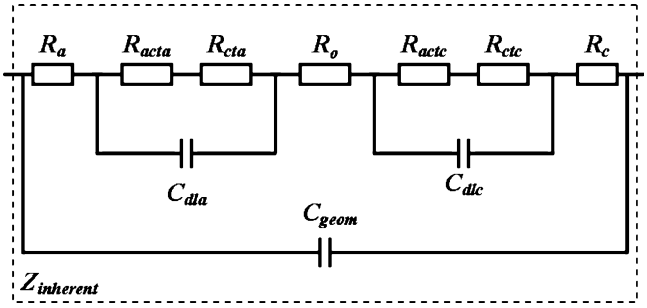

Fig. 3. Equivalent circuit of inherent impedance.

(1) Three types of resistances representing the ohmic resistances (R_{o}, R_{a}, R_{c}) the activation resistances (R_{acta}, R_{actc}) and the charge transfer resistances (R_{cta}, R_{ctc}).
(2) Two charge capacities (C_{dla}, C_{dlc}) due to the double layer phenomenon and one geometrical capacity C_{geom} between the electrodes. Indeed, the structure of charge accumulation and the charge separation always occur at the interface when an electrode is immersed into an electrolyte solution. The excess charge on the electrode surface is compensated by an accumulation of excess ions of the opposite charge in the solution. This structure behaves essentially as capacitor and leads to (C_{dla}, C_{dlc}). For C_{geom}, it follows from the fact that two electrodes (anode, cathode) separated with an isolator (electrolyte) produce a capacitance effect between them.

In fact, the inherent impedance Z_{inherent} is modeled as an equivalent RC circuit. A typical equivalent circuit which takes into account all inherent impedances is shown in Fig. 3.

Introducing the electrochemical reaction potential and the load resistance to the inherent impedance we obtain the equivalent circuit of the PEMFC shown in Fig. 4, where i_{c} is the current of the geometrical capacity. The model shown in Fig. 4

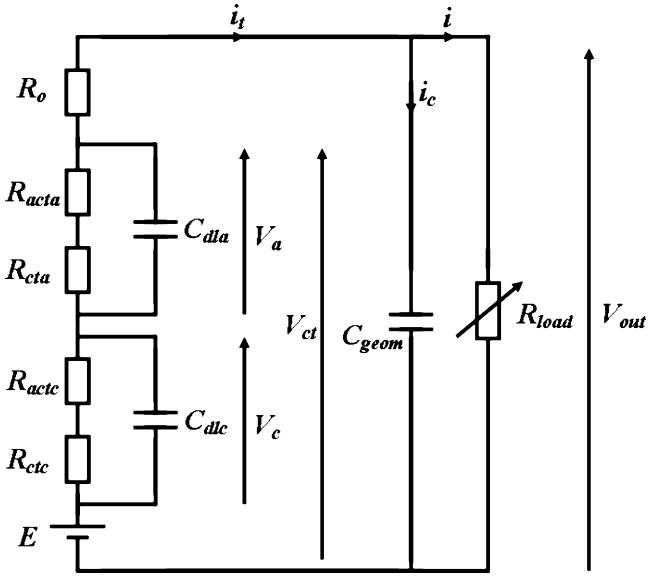

Fig. 4. Equivalent circuit of one cell.

is an integral circuit that appears to be realistic by introducing activation, ohmic and concentration losses as well as the double layer and geometrical capacitance effects. Resistances are calculated with respect to the inputs while capacities can be identified from impedance spectral plan plot [11].

Let V_e be either V_a or V_c. According to Ohm's law, the expression of V_e from the equivalent circuit is as follows:

$$V_e = -(R_{act} + R_{ct}) \left[i_t + C_{dl} \frac{dV_e}{dt} \right]. \tag{20}$$

This implies that:

$$\frac{dV_e}{dt} = \frac{-1}{(R_{act} + R_{ct})C_{dl}} V_e - \frac{1}{C_{dl}} i_t. \tag{21}$$

Therefore, the voltage and current outputs are calculated as follows:

$$\begin{aligned} V_{ct} &= E + 2V_e \\ V_{out} &= V_{ct} - i_t R_0 = E + 2V_e - i_t R_0 \\ i_t &= i + i_c = \frac{V_{out}}{R_{load}} + C_{geom} \frac{dV_{out}}{dt}. \end{aligned} \tag{22}$$

This leads to:

$$V_{out} = E + 2V_e - R_0 \left[\frac{V_{out}}{R_{load}} + C_{geom} \frac{dV_{out}}{dt} \right]. \tag{23}$$

The solution of Eq. (23) with respect to the initial condition $V_{out}(0) = 0$ gives:

$$V_{out}(t) = \frac{R_{load}(E + 2V_e)[1 - \exp(-((R_{load} + R_o)/R_{load}R_o C_{geom})t)]}{R_{load} + R_o} \tag{24}$$

3.3. State-space representation

In this part, we present the model based on diffusional and electrical approaches in the state-space form. In order to model the dynamic behavior of gas consumption rates, we convert the transfer function form the dynamic relations shown in Eq. (18) to a differential equation form as follows:

- Hydrogen consumption rate:

$$\ddot{J}^s_{H_2} = -\alpha_1 J^s_{H_2} - \alpha_2 \dot{J}^s_{H_2} + \alpha_1 J^r_{H_2} + \alpha_3 \frac{A}{R_g T} \dot{p}^b_{H_2}$$

and its partial pressure in the vicinity of anode at TPB:

$$\ddot{p}^{tpb}_{H_2} = -\alpha_1 p^{tpb}_{H_2} - \alpha_2 \dot{p}^{tpb}_{H_2} - \alpha_4 \frac{R_g T}{A} J^r_{H_2} - \frac{4}{L_a} \frac{R_g T}{A} \dot{J}^r_{H_2} + \alpha_1 p^b_{H_2}$$

where $\alpha_1 = 24D^2_{H_2}/L^4_a$, $\alpha_2 = 12D_{H_2}/L^2_a$, $\alpha_3 = 24D^2_{H_2}/L^3_a$, $\alpha_4 = 24D_{H_2}/L^3_a$.

- Oxygen consumption rate:

$$\ddot{J}^s_{O_2} = -\beta_1 J^s_{O_2} - \beta_2 \dot{J}^s_{O_2} + \beta_1 J^r_{O_2} + \beta_3 \frac{A}{R_g T} \dot{p}^b_{O_2}$$

and its partial pressure in the vicinity of cathode at TPB:

$$\ddot{p}^{tpb}_{O_2} = -\beta_1 p^{tpb}_{O_2} - \beta_2 \dot{p}^{tpb}_{O_2} - \beta_4 \frac{R_g T}{A} J^r_{O_2} - \frac{4}{L_c} \frac{R_g T}{A} \dot{J}^r_{O_2} + \beta_1 p^b_{O_2}$$

where $\beta_1 = 24D^2_{O_2}/L^4_c$, $\beta_2 = 12D_{O_2}/L^2_c$, $\beta_3 = 24D^2_{O_2}/L^3_c$, $\beta_4 = 24D_{O_2}/L^3_c$.

- Water vapor production rate:

$$\ddot{J}^s_{H_2O} = -\gamma_1 J^s_{H_2O} - \gamma_2 \dot{J}^s_{H_2O} + \gamma_1 J^r_{H_2O} + \gamma_3 \frac{A}{R_g T} \dot{p}^b_{H_2O}$$

and its partial pressure in the vicinity of anode at TPB:

$$\ddot{p}^{tpb}_{H_2O} = -\gamma_1 p^{tpb}_{H_2O} - \gamma_2 \dot{p}^{tpb}_{H_2O} - \gamma_4 \frac{R_g T}{A} J^r_{H_2O} - \frac{4}{L_a} \frac{R_g T}{A} \dot{J}^r_{H_2O} + \gamma_1 p^b_{H_2O}$$

where $\gamma_1 = 24D^2_{H_2O}/L^4_a$, $\gamma_2 = 12D_{H_2O}/L^2_a$, $\gamma_3 = 24D^2_{H_2O}/L^3_a$, $\gamma_4 = 24D_{H_2O}/L^3_a$.

The above equations show that gases consumption rates depend on input derivatives ($\dot{u}_2$, $\dot{u}_3$ and $\dot{u}_4$). This fact is generally negative because the derivative mode can amplify the outputs noise. Therefore, we use a low-pass filter to eliminate the noise increasing in derivative mode. Consequently, the first order derivative of the input variables can be approximated by the following equation [16]:

$$sU(s) \approx K \left(1 - \frac{1}{1 + s/K} \right) U(s),$$

where K is an approximation factor greater than 10. Let v be an auxiliary input defined as $v(s) = (1/(1 + s/K))U(s)$. Then we have:

$$\begin{aligned} \dot{u} &= Ku - v \\ \dot{v} &= K^2 u - Kv \end{aligned}$$

Hence, after introducing the intermediate variables v_{H_2}, v_{O_2}, v_{H_2O} and $v_{R_{load}}$ to the model, we define the state-space vector as follows:

$$x = [V_e, p^{tpb}_{H_2}, p^{tpb}_{O_2}, p^{tpb}_{H_2O}, \dot{P}^{tpb}_{H_2}, \dot{P}^{tpb}_{O_2}, \dot{P}^{tpb}_{H_2O}, J^s_{H_2}, \dot{J}^s_{H_2}, v_{H_2}, J^s_{O_2}, \dot{J}^s_{O_2}, v_{O_2}, J^s_{H_2O}, \dot{J}^s_{H_2O}, v_{H_2O}, v_{R_{load}}]^T$$

This together with all the above equations lead to the following state-space model:

$$\begin{aligned} \dot{x}_1 &= -\frac{x_1}{(R_{act} + R_{ct})C_{dl}} - \frac{i_t}{C_{dl}} \\ \dot{x}_2 &= x_5; \\ \dot{x}_3 &= x_6; \\ \dot{x}_4 &= x_7; \\ \dot{x}_5 &= -\alpha_1 x_2 + \alpha_1 u_2 - \alpha_2 x_5 - \alpha_4 \frac{R_g u_6}{2FA} i_t - \frac{2R_g u_6}{FAL_a} \frac{di_t}{dt}; \\ \dot{x}_6 &= -\beta_1 x_3 + \beta_1 u_3 - \beta_2 x_6 - \beta_4 \frac{R_g u_6}{4FA} i_t - \frac{R_g u_6}{FAL_c} \frac{di_t}{dt}; \end{aligned}$$

$$\dot{x}_7 = -\gamma_1 x_4 + \gamma_1 u_4 - \gamma_2 x_7 - \gamma_4 \frac{R_g u_6}{2FA} i_t - \frac{2R_g u_6}{FAL_a} \frac{di_t}{dt};$$

$$\dot{x}_8 = x_9;$$

$$\dot{x}_9 = -\alpha_1 x_8 - \alpha_2 x_9 + \frac{\alpha_1}{2F} i_t + \frac{\alpha_3 A}{R_g u_6}(Ku_2 - x_{10});$$

$$\dot{x}_{10} = K^2 u_2 - K x_{10};$$

$$\dot{x}_{11} = x_{12};$$

$$\dot{x}_{12} = -\beta_1 x_{11} - \beta_2 x_{12} + \frac{\beta_1}{4F} i_t + \frac{\beta_3 A}{R_g u_6}(Ku_3 - x_{13});$$

$$\dot{x}_{13} = K^2 u_3 - K x_{13};$$

$$\dot{x}_{14} = x_{15};$$

$$\dot{x}_{15} = -\gamma_1 x_{14} - \gamma_2 x_{15} + \frac{\gamma_1}{2F} i_t + \frac{\gamma_3 A}{R_g u_6}(Ku_4 - x_{16});$$

$$\dot{x}_{16} = K^2 u_4 - K x_{16};$$

$$\dot{x}_{17} = K^2 u_1 - K x_{17}.$$

The output equations are represented as follows:

$$y_1 = \frac{u_1(E + 2x_1)[1 - \exp(-((u_1 + R_o)/u_1 R_o C_{geom})t)]}{u_1 + R_o};$$

$$y_2 = \frac{y_1}{u_1}; \quad y_3 = x_8; \quad y_4 = x_{11}; \quad y_5 = x_{14}.$$

Here, the variables i_t, di_t/dt, R_{act}, R_{ct}, E and R_o are as follows:

$$i_t = \frac{(E + 2x_1)[1 - \exp(-((u_1 + R_o)/u_1 R_o C_{geom})t)]}{u_1 + R_o} + \frac{(E + 2x_1)[\exp(-((u_1 + R_o)/u_1 R_o C_{geom})t)]}{R_o}$$

$$\frac{di_t}{dt} = \frac{(E + 2x_1)[\exp(-((u_1 + R_o)/u_1 R_o C_{geom})t)]}{u_1 R_o C_{geom}} - \frac{(E + 2x_1)(u_1 + R_o)[\exp(-((u_1 + R_o)/u_1 R_o C_{geom})t)]}{u_1 R_o^2 C_{geom}}$$

$$R_{act} = \frac{Ru_6}{2i_t F} \ln\left(\frac{i_t}{i_0}\right);$$

$$R_{ct} = \frac{Ru_6}{2i_t F} \ln\left(1 - \frac{i_t}{i_l}\right);$$

$$E = E^0 + \frac{R_g u_6}{2F} \ln\left(\frac{x_2\sqrt{x_3}}{x_4}\right);$$

$$R_o = R_a + R_c + R_m;$$

$$R_m = \frac{L_m}{\sigma A};$$

$$\sigma = (5139 \times 10^{-6} u_5 - 326 \times 10^{-5})\, e^{1268((1/303)-(1/u_6))}.$$

Hence, the state-space model is developed in the following form:

$$\dot{x} = f(x, u, t)$$
$$y = g(x, u, t)$$

This form is a non-linear dynamic model which is essential for the optimal operation and the control of many processes. It presents a powerful tool for simulating the real behavior of the system because the state-space form allows a detailed analysis of the cell temporal and spatial behavior. The temporal behavior provides the evolution of all state variables with respect to the time axis while the spatial behavior provides a so-called phase space which consists on the representation of some or all state variables in a multidimensional space. This phase space may give qualitative information about the dynamics of the system. In addition, the state-space form is suitable for the optimization of physical parameters and is well suited for synthesis of a controller to stabilize the cell voltage or reject the possible environmental disturbances.

4. Simulation results

In this section, we will present the simulation results that demonstrate the effect of the load change and its disturbance, the gas pressures change as well as the effects of humidification and temperature. The simulation is done according to the developed model and it investigates steady-state and transient behaviors of a single cell at different inputs and disturbances. It is done under Matlab-Simulink using the well known S-function toolbox as shown in Fig. 5.

Since data related to dynamic models are limited in the literature, we will simulate the model according to the parameters of [11,12]. Most of these data are taken from [11] because the author studies the PEMFC. However, some other parameters are taken from [12] like the cell dimension (A, L_a, L_c) and the porous characteristics of the electrodes (ϵ, τ). The simulation results represent the dynamic behavior for one cell of PEMFC. The parameter values are shown in Table 2.

4.1. Effect of load

The load is usually imposed by the external circuit. However, we consider it as an input in order to view the effect of its change on the outputs. We will present its effect by simulating the responses to pulse, triangular and sinusoidal resistance change as well as the effect of the disturbance (Figs. 6–11).

One can immediately observe that the variation of the current is opposite to the variation of the load resistance while the output voltage change is proportional to it. This is in agreement with Eq. (22). In addition, we notice that the current variation is bigger comparing to the voltage one, this is due to the fact that the influence of the load on the current is larger than its influence on the voltage. Indeed, from Eqs. (22) and (24) we have:

$$i = \frac{V_{out}}{R_{load}},$$

$$V_{out}(t) = \frac{R_{load}(E + 2V_e)[1 - \exp(-((R_{load} + R_o)/R_{load} R_o C_{geom})t)]}{R_{load} + R_o} \quad (25)$$

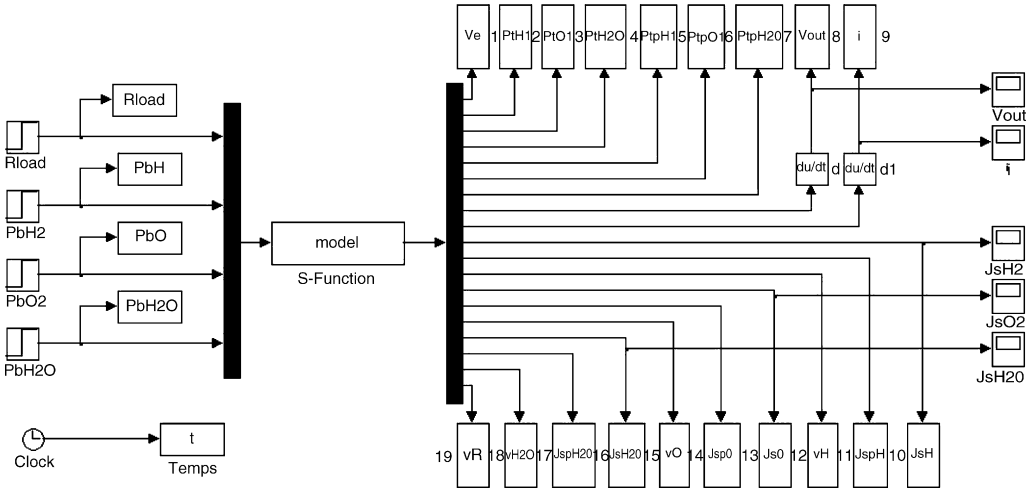

Fig. 5. Simulink model.

Table 2
Parameters value

Symbol	Description	Symbol	Description
$A = 1\,\text{cm}^2$	Fuel cell effective area	$p^{\text{b}}_{\text{H}_2} = 2.5 \times 10^5\,\text{Pa}$	Hydrogen partial pressure in anode gas bulk
$C_{\text{dl}} = 186\,\text{mF}$	Double layer capacitance	$p^{\text{b}}_{\text{O}_2} = 2.5 \times 10^5\,\text{Pa}$	Oxygen partial pressure in cathode gas bulk
$C_{\text{geom}} = 186\,\text{mF}$	Geometrical capacitance	$p^{\text{b}}_{\text{H}_2\text{O}} = 1 \times 10^5\,\text{Pa}$	Water partial pressure in cathode gas bulk
$\epsilon = 0.4$	Porosity	$R_{\text{a}} = 45\,\text{m}\Omega$	Anode resistance
$i_0 = 0.2\,\text{A}$	Activation current	$R_{\text{c}} = 45\,\text{m}\Omega$	Cathode resistance
$i_{\text{l}} = 2\,\text{A}$	Limit current	$r = 20\,\mu\text{m}$	Pore radius
$L_{\text{a}} = 1\,\text{mm}$	Thickness of anode diffusion layer	$\tau = 4$	Tortuosity
$L_{\text{c}} = 1\,\text{mm}$	Thickness of cathode diffusion layer		
$L_{\text{m}} = 0.2\,\text{mm}$	Thickness of membrane		

Because $R_{\text{o}} \ll R_{\text{load}}$ we have $R_{\text{o}} + R_{\text{load}} \approx R_{\text{load}}$. Given this fact, the expression of V_{out} becomes:

$$V_{\text{out}}(t) \approx \frac{R_{\text{load}}(E + 2V_{\text{e}})[1 - \exp(-(R_{\text{load}}/R_{\text{load}}R_{\text{o}}C_{\text{geom}})t)]}{R_{\text{load}}}$$

$$= (E + 2V_{\text{e}})\left[1 - \exp\left(-\frac{t}{R_{\text{o}}C_{\text{geom}}}\right)\right]. \quad (26)$$

Hence, one can immediately observe from Eqs. (25) and (26) that the load influence on the current is more important than its influence on the voltage.

Furthermore, simulations in Fig. 6 show that the time response between the input change and the output responses is about 0.25 s (see Fig. 9). Comparing this result with one presented in [12], where the time response is 0.08 s, we see that the difference is due to the fact that in our study we take into

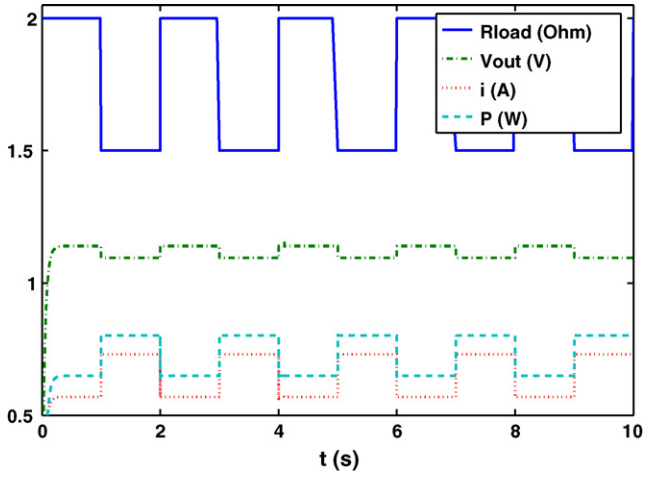

Fig. 6. Responses to pulse load changes.

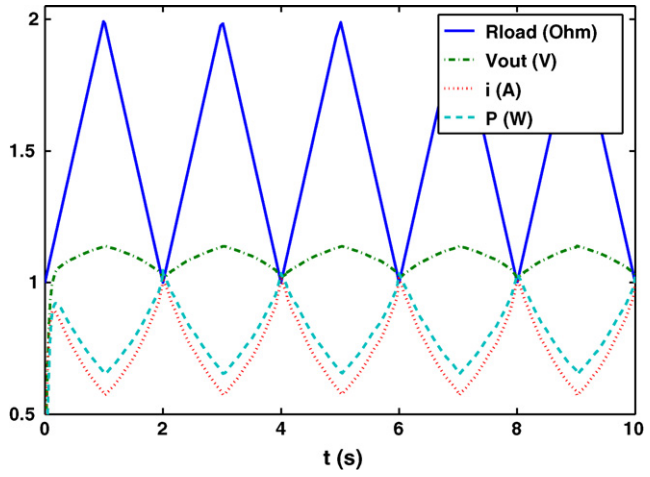

Fig. 7. Responses to triangular load changes.

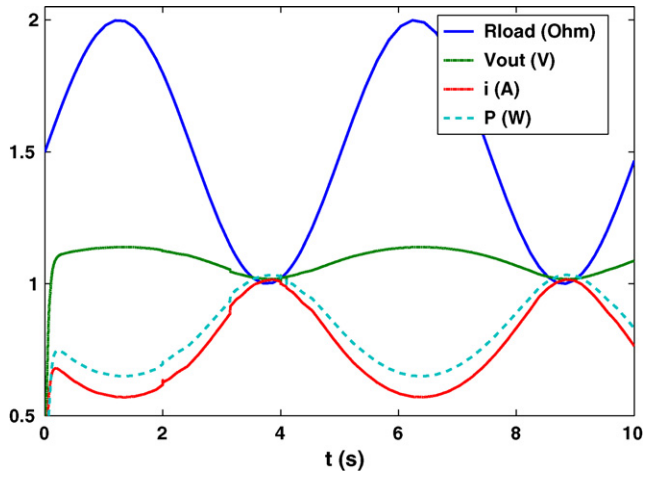

Fig. 8. Responses to sinusoidal load changes.

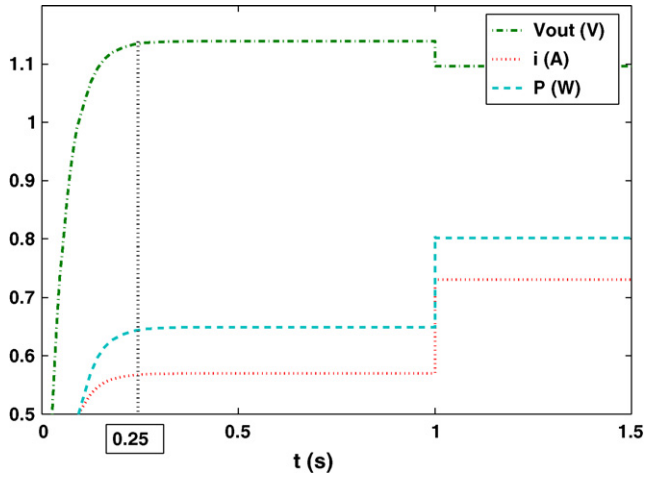

Fig. 9. Time response of the outputs.

account the effect of the geometrical capacity while the work of [12] do not consider it.

As in [12,11], we do not have any overflow in the output responses. This is related to the input values. In general, the overflow is proportional to the velocity of the load variation.

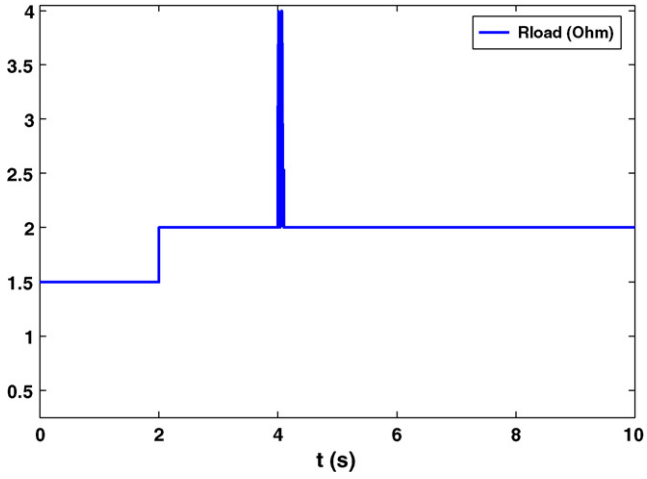

Fig. 10. Load disturbance.

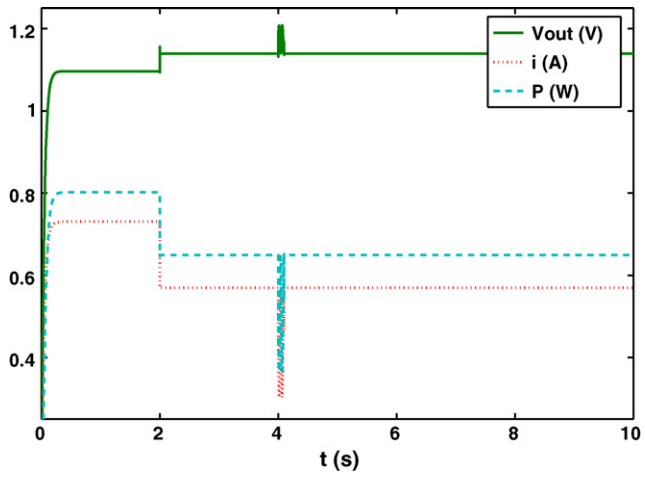

Fig. 11. Responses to load disturbance.

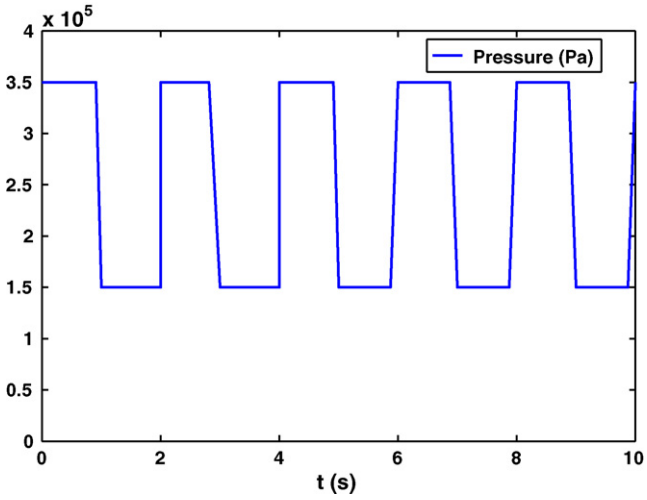

Fig. 12. Gase pressure change.

The results of Fig. 11 show the effect of the load disturbance (Fig. 10) on current and voltage.

One can observe that variables are immediately influenced by load disturbance, but the current is more disturbed than the volt-

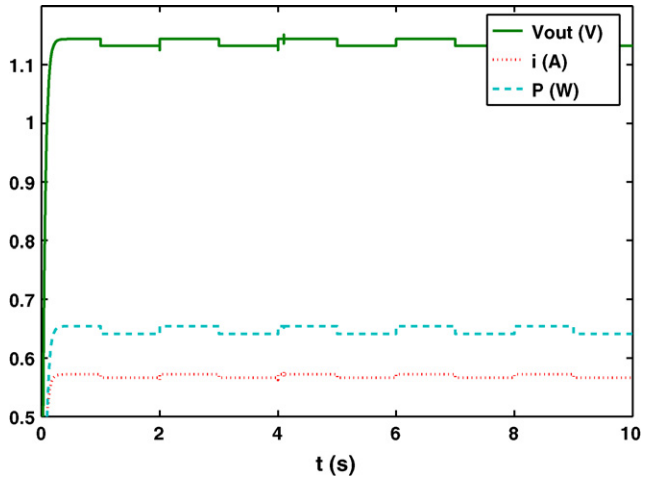

Fig. 13. Responses to hydrogen pressure pulse.

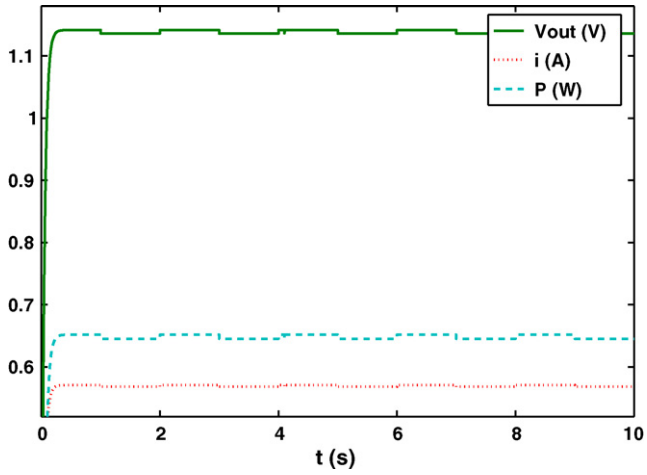

Fig. 14. Responses to oxygen pressure pulse.

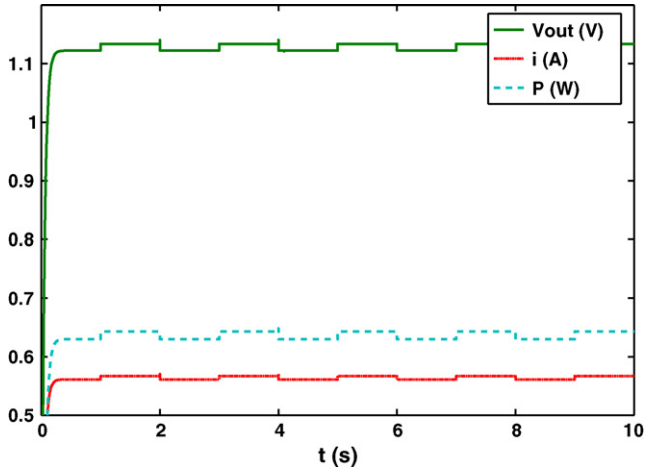

Fig. 15. Responses to water pressure pulse.

age because the load influence on the former is more important than its influence on the latter (see explanation in this section). For a load disturbance of 100%, the current change is about 50% while the voltage one is about 4%.

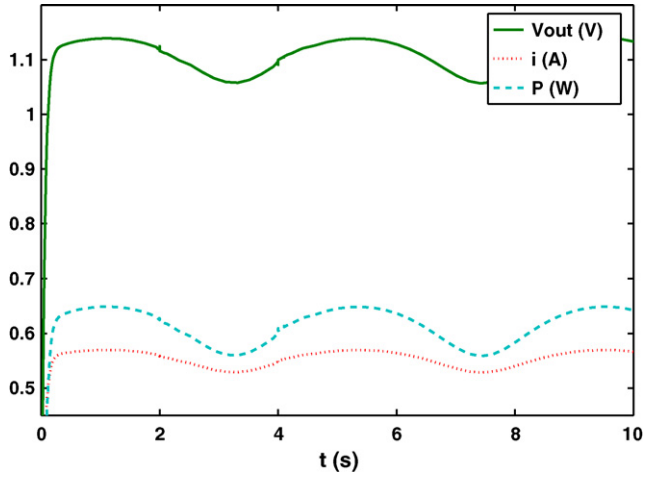

Fig. 16. Effect of membrane humidity.

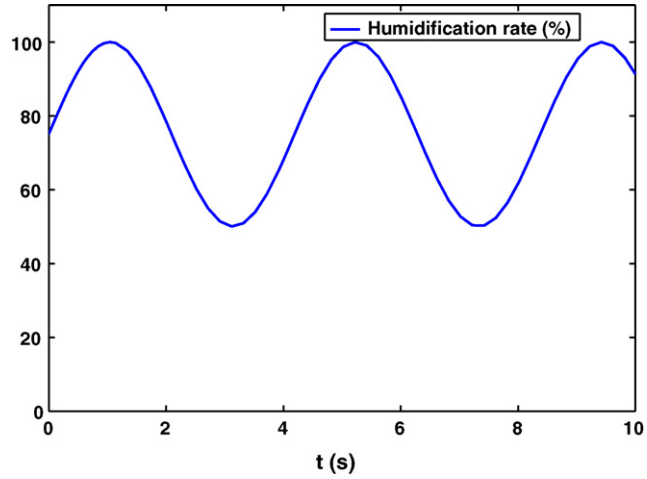

Fig. 17. Membrane humidification rate change.

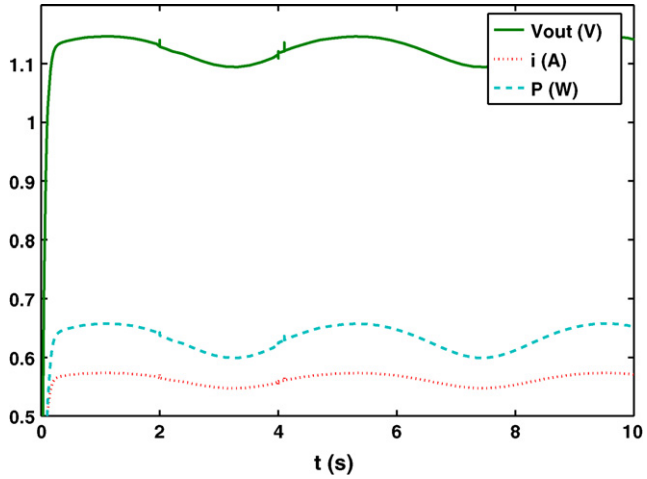

Fig. 18. Effect of temperature.

4.2. *Effect of partial pressures*

Usually, the control of the fuel cell system is not based on reactant pressure action, because this parameter does not have a big influence on the outputs. This fact will be shown in this part

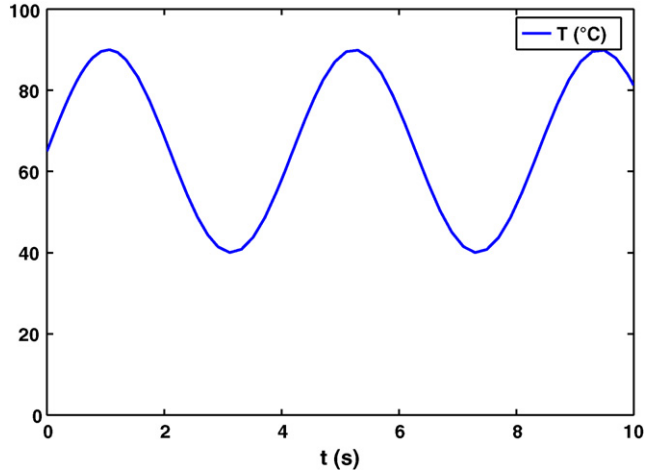

Fig. 19. Temperature change.

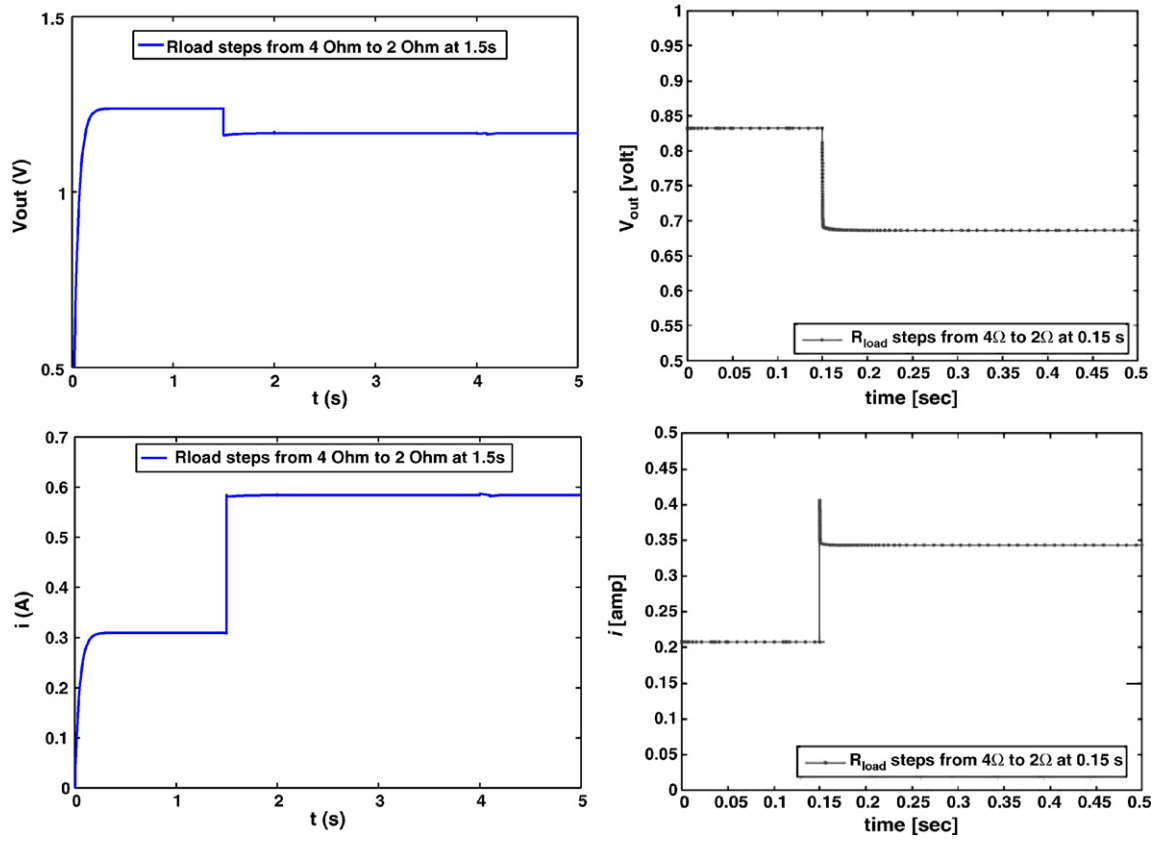

Fig. 20. Response to R_{load} steps from 4 to 2 Ω.

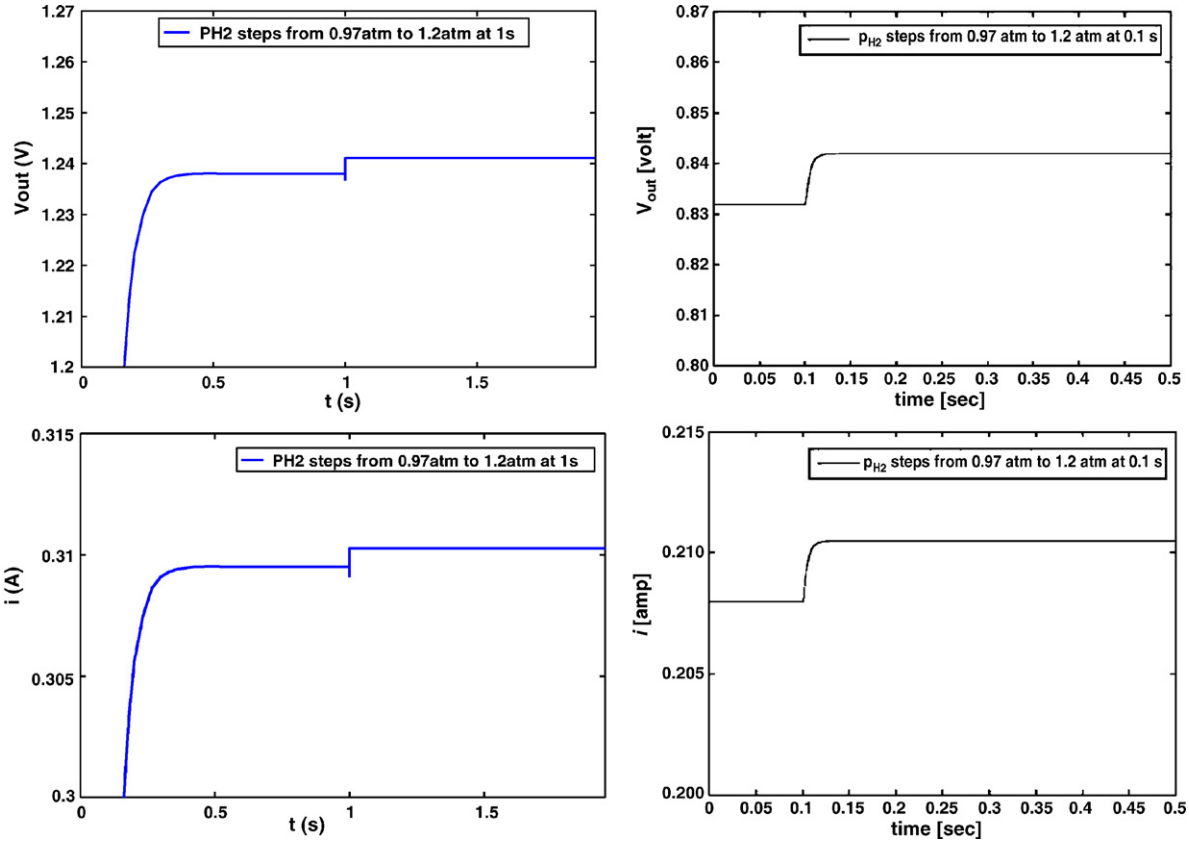

Fig. 21. Response to p_{H_2} steps from 0.97 to 1.2 atm.

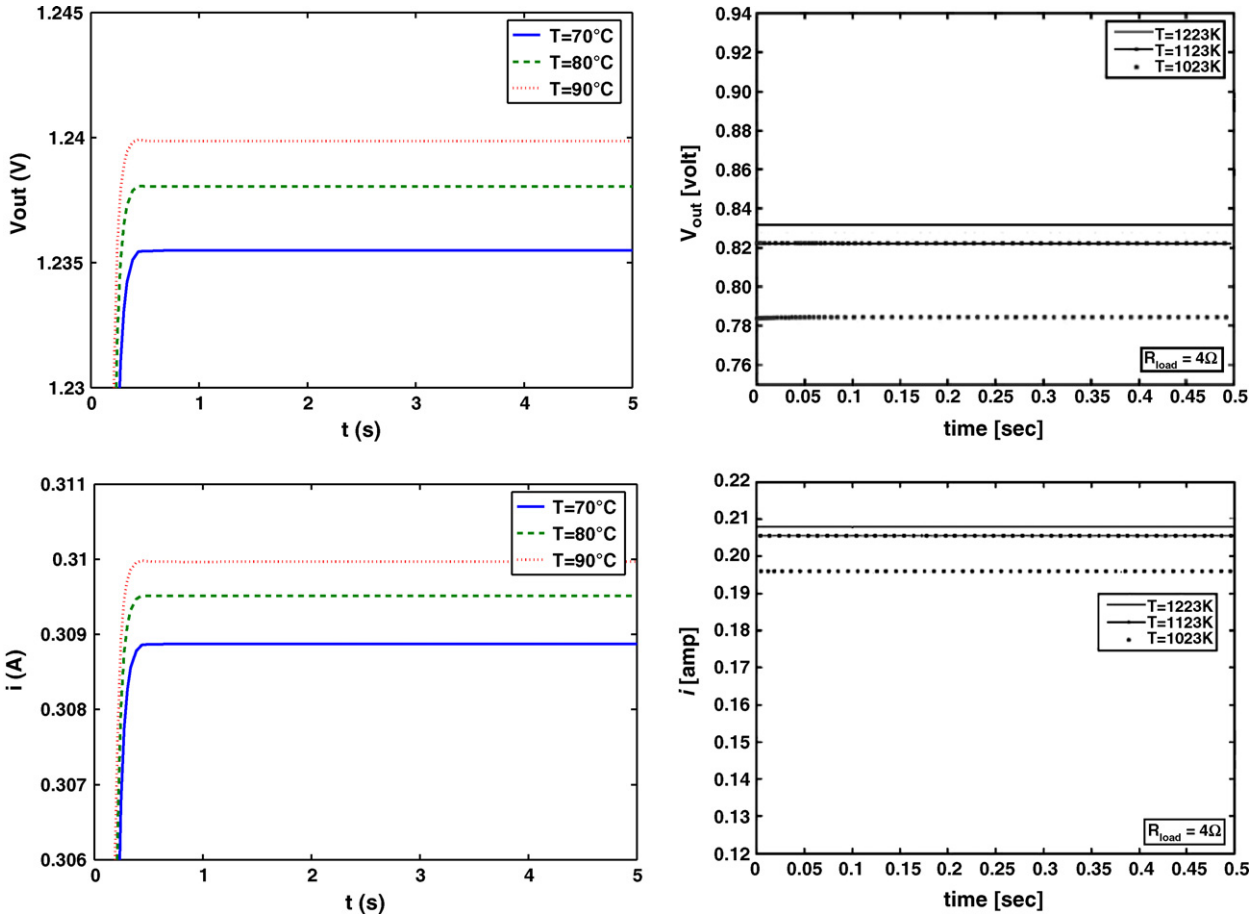

Fig. 22. Effect of temperature.

where we simulate the effect of hydrogen, oxygen and water pressures by simulating the output responses to pulse pressure change (Fig. 12).

According to Nernst equation, we see in Figs. 13–15 that the voltage response is proportional to hydrogen and oxygen pressure evolutions but it is conversely proportional to the water pressure. Comparing Figs. 13–15, we observe that the variation of the voltage output with respect to $p^{b}_{H_2O}$ and $p^{b}_{H_2}$ is more important than its variation with respect to $p^{b}_{O_2}$. This is coherent with the fuel cell principle because cathode reaction is slower than anode one.

4.3. Effect of humidification

As described before, the effect of the membrane humidity is very important because it influences the loss behavior. Indeed, the membrane humidity affects its resistance value which is the main element that determines the ohmic loss. The simulation results in Fig. 16 show the output responses to the humidification rate change (Fig. 17) between 50 and 100%. One can show that the voltage V_{out} and the current i behave proportionally to the humidification rate λ_m. This is due to the fact that the membrane resistance R_m is conversely proportional to λ_m.

4.4. Effect of temperature

The fuel cell temperature is an important factor that influences the outputs because it affects the Nernst voltage as well as the activation, ohmic and concentration resistances. The simulation results in Fig. 18 show the outputs responses to the temperature change (Fig. 19) between 40 and 90 °C.

According to Eqs. (3) and (22), we can see in Fig. 18 that both voltage and current are proportional to the temperature. This is due to the fact that Nernst voltage and membrane resistance are proportional to the temperature.

In conclusion, we can emphasize the fact that the dynamic behavior of the fuel cell outputs is mainly influenced by the fuel cell temperature, the humidification of the membrane and the external load.

5. Comparison with other work

As we mentioned in the introduction, most of the work in the literature are centered on either static electrochemical aspect or linear dynamic aspect. With the best of our knowledge, the notable work which takes into account the non-linearity aspect is the one presented in [12]. However, the paper focuses on the solid oxide fuel cell and do not take into account the activation loss,

the geometrical capacity as well as the evolution of some important variables like the fuel cell temperature and the membrane humidity. In addition, we do not have the same functional conditions, for instance, the functional temperature for the PEMFC is 80 °C while it is 800 °C for the SOFC. For all these reasons, our output values are different comparing to those presented in [12] but nevertheless they must have the same behavior due to the fuel cell principle. The comparison diagrams show the behavior similarity of V_{out} and i with respect to R_{load}, p_{H_2} and T change in both cases. The only important point that should be noted is that in our results (Figs. 20–22, left side) the overflow appears at the pressure response contrarily to the results of [12] (Figs. 20–22, right side) which appears at R_{load} response. Besides, we do not consider the same time scale because we have a bigger time response.

6. Conclusion

In this paper, a non-linear dynamical state-space model of planar proton exchange membrane fuel cell has been built. In our model, we have considered the majority of the phenomena that influence the dynamic behavior of the fuel cell. In particular, a realistic equivalent circuit has been proposed. In that circuit, we have considered all the fuel cell elements that cause the energy losses. Furthermore, the pressure effect on the electrochemical reaction potential as well as the one of the temperature and the humidification rate on resistances have been also taken into account. Simulation results show that the main elements that influence the outputs are temperature, humidification rate and load. Hence, our model is in agreement with the fuel cell principle.

In conclusion, with the aid of dynamical model, there are several issues that deserve further investigation. One is the control of the energy losses in the fuel cell. Indeed, among the real obstacles (such as production costs and life limitations) for fuel cells to become a success is their energy losses. This problem is even more accentuated for automotive applications because the energy loss lies at the core of performance problems. The performance of a fuel cell depends not only on the individual components but also on how the components are controlled. Hence, minimizing energy losses can be applied to the model using methods from optimal control. This is a topic of our future research.

Acknowledgment

The authors would like to thank the referees for their careful reviews and suggestions in the improvement of the paper.

References

[1] F. Barbir, B. Balasubramanian, J. Neutzler, Proceedings of the ASME Advanced Energy Systems Division 39, 1999, pp. 305–315.
[2] D.D. Boettner, G. Paganelli, Y.G. Guezennec, G. Rizzoni, M.J. Moran, Proceedings of 2001 ASME International Mechanical Engineering Congress and Exposition, 2001.
[3] G. Shan-Hai, Y. Bao-Lian, J. Power Sources 124 (2003) 1–11.
[4] D.J. Friedman, A. Egghert, P. Badrinarayanan, J. Cunningham, Balancing stack, air supply and water/thermal management demands for an indirect methanol PEM fuel cell system, SAE Paper 2001-01-0535.
[5] S. Akella, N. Sivashankar, S. Gopalswamy, Proceedings of 2001 American Control Conference, 2001.
[6] J. Pukrushpan, H. Peng, A. Stefanopoulou, J. Dyn. Syst. Meas. Control 126 (2004) 14–25.
[7] L. Guzzella, A. Amstutz, IEEE Trans. Vehicular Technol. 48 (1999) 1762–1769.
[8] S. Busquet, C.E. Hubert, J. Labbe, D. Mayer, R. Metkemeijer, J. Power Sources 134 (2004) 41–48.
[9] F. Standaert, K. Hemmes, N. Woudstra, J. Power Sources 63 (1996) 221–234.
[10] J. Lachaize, Etude des stratégies et des structures de commande pour le pilotage des systèmes énergétiques à pile à combustible destinés à la traction, Ph.D. Thesis, Laboratoire d'Electrotechnique et d'Electronique Industrielle de l'ENSEEIHT, Toulouse, 2004.
[11] R. Saisset, Contribution à l'étude systémique de dispositifs énergétiques à composants électrochimiques, Ph.D. Thesis, Laboratoire d'Electrotechnique et d'Electronique Industrielle de l'ENSEEIHT, Toulouse, 2004.
[12] Y. Qi, B. Huang, K. Chuang, J. Power Sources 150 (2005) 32–47.
[13] S. Campanari, P. Iora, J. Power Sources 132 (2004) 113–126.
[14] S. Caux, J. Lachaize, M. Fadel, P. Shott, L. Nicod, J. Process Control 15 (2005) 481–491.
[15] J. Golbert, D. Lewin, J. Power Sources 135 (2003) 135–151.
[16] D.E. Seborg, T.F. Edgar, D.A. Mellichamp, Process Dynamics and Control, first ed., John Wiley and Sons Inc., 1989.